An interactive atlas of three-dimensional syndromic facial morphology

Authors

J. David Aponte, Jordan J. Bannister, Hanne Hoskens, ..., Ophir D. Klein, David C. Katz, Benedikt Hallgrímsson

Correspondence

bhallgri@ucalgary.ca

We present an online tool for visualizing 3D facial shape variation associated with 95 different genetic syndromes. Our tool allows visualization of variation in severity as well as modulation of facial shape effects with age and by sex. This tool can serve as a diagnostic reference and for training.

Aponte et al., 2024, The American Journal of Human Genetics *111*, 39–47
January 4, 2024
https://doi.org/10.1016/j.ajhg.2023.11.011

CellPress

An interactive atlas of three-dimensional syndromic facial morphology

J. David Aponte,[1,2] Jordan J. Bannister,[2] Hanne Hoskens,[1] Harold Matthews,[3] Kaitlin Katsura,[4] Cassidy Da Silva,[1] Tim Cruz,[2] Julie H.M. Pilz,[2] Richard A. Spritz,[5] Nils D. Forkert,[6] Peter Claes,[3,7] Francois P. Bernier,[8] Ophir D. Klein,[4,9] David C. Katz,[1,2] and Benedikt Hallgrímsson[1,*]

Summary

Craniofacial phenotyping is critical for both syndrome delineation and diagnosis because craniofacial abnormalities occur in 30% of characterized genetic syndromes. Clinical reports, textbooks, and available software tools typically provide two-dimensional, static images and illustrations of the characteristic phenotypes of genetic syndromes. In this work, we provide an interactive web application that provides three-dimensional, dynamic visualizations for the characteristic craniofacial effects of 95 syndromes. Users can visualize syndrome facial appearance estimates quantified from data and easily compare craniofacial phenotypes of different syndromes. Our application also provides a map of morphological similarity between a target syndrome and other syndromes. Finally, users can upload 3D facial scans of individuals and compare them to our syndrome atlas estimates. In summary, we provide an interactive reference for the craniofacial phenotypes of syndromes that allows for precise, individual-specific comparisons of dysmorphology.

Introduction

Most syndrome diagnoses are initially based on clinical assessment. Craniofacial phenotypes are central to a large fraction of those assessments because craniofacial abnormalities are present in 30% of known genetic syndromes.[1] It is left to the clinician, over many years of training and patient encounters, to develop their own sense of how syndromic phenotypes vary. While definitive molecular diagnoses are theoretically possible, they are expensive, frequently not practically available, and even when available are not always diagnostically conclusive.[2–6] As a result, adjunct tools to facilitate and enhance clinical impressions are highly valuable and are likely to continue to play a prominent role in diagnosis for the foreseeable future.

Characteristic craniofacial phenotypes of genetic syndromes have been extensively documented in case reports, books, and web resources using facial images of patients or representative drawings.[7,8] Although useful as a reference, a static image can only capture an individual or, at best, an average syndromic phenotype for a specific age, sex, ethnicity, and body type. Individuals with a specific diagnosis, however, can exhibit wide phenotypic variation depending on these same metrics. Bias can also be introduced from illustrations in cases where highlighting or exaggerating features does not take into account that other features of the face will tend to correlate with those features and so should also be changed accordingly. This tendency to overlook the integrated nature of facial shape variation can result in illustrations that do not accurately reflect the typical syndrome phenotype. Finally, clinical illustrations do not typically focus on phenotypic heterogeneity or demographic influences, which are observed in virtually all craniofacial syndromes.[9] As an example, Figure 1A highlights the range of syndromic facial features in a sample of 50 individuals with achondroplasia.

Fortunately, adjusting characteristic phenotypes for demographic influences is a natural application of quantitative analysis. A number of studies have demonstrated the utility of statistical approaches to generating demographically specific estimates of syndromic facial form.[10,11] Several studies have taken a quantitative approach to characterizing syndromic facial phenotypes by deriving facial shape measurements from 2D or 3D images and estimating a mean shape.[12,13] An alternative method is to produce a 2D or 3D "facial archetype" or "gestalt."[13] Figure 1B demonstrates an average image for achondroplasia (MIM: 100800). Modifying these facial archetypes to illustrate demographically specific syndromic representations then becomes a matter of acquiring a dataset of sufficient diversity.

Shape and facial archetype approaches have also been used for 3D syndromic facial data.[14,15] As with 2D

[1]Department of Cell Biology & Anatomy, Alberta Children's Hospital Research Institute and McCaig Bone and Joint Institute, Cumming School of Medicine, University of Calgary, Calgary, AB, Canada; [2]DeepSurface AI Inc., Calgary, AB, Canada; [3]Department of Human Genetics, KU Leuven, Leuven, Belgium; [4]Department of Orofacial Sciences and Program in Craniofacial Biology, University of California, San Francisco, San Francisco, CA, USA; [5]Department of Pediatrics and the Human Medical Genetics and Genomics Program, University of Colorado School of Medicine, Aurora, CO, USA; [6]Department of Radiology and Alberta Children's Hospital Research Institute, Cumming School of Medicine, University of Calgary, Calgary, AB, Canada; [7]Department of Electrical Engineering, ESAT/PSI, KU Leuven, Leuven, Belgium; [8]Department of Medical Genetics and the Alberta Children's Hospital Research Institute, University of Calgary, Calgary, AB, Canada; [9]Department of Pediatrics, Cedars-Sinai Guerin Children's, Los Angeles, CA, USA
*Correspondence: bhallgri@ucalgary.ca
https://doi.org/10.1016/j.ajhg.2023.11.011.

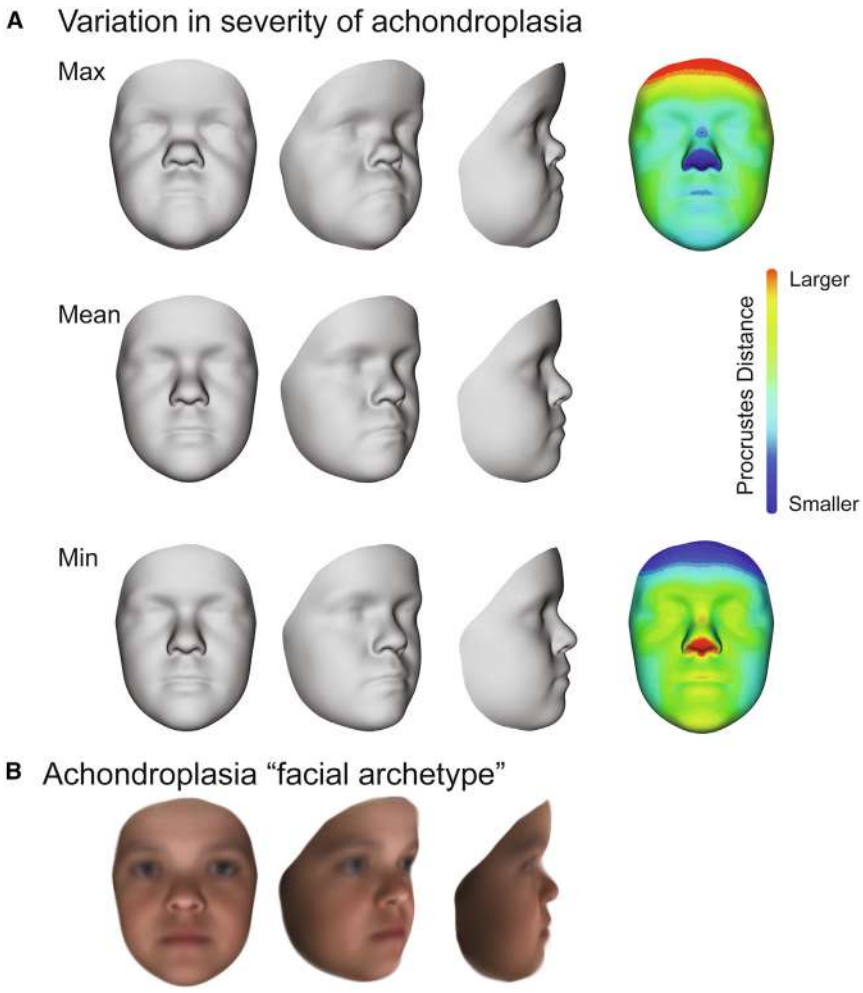

Figure 1. Syndromic heterogeneity and measurements of syndromic gestalts using achondroplasia as an example

(A) The most-severe, average, and least-severe shape gestalts from a sample of 50 individuals with achondroplasia. Heatmaps represent the per-vertex deformation relative to the achondroplasia mean shape.

(B) An image of "facial archetype" generated with non-linear deformation of 2D screenshots to the achondroplasia mean.

landmarks, 3D landmarks allow the positions and deviations of characteristic features to be measured. With 3D scans, facial archetypes can be described with visualizations of average 3D meshes as well as facial heatmaps. Compared to 2D image averages, 3D visualizations can better represent differences in depth, which may better match what the clinician observes meeting with patients (Figure 1A).

Such quantitative studies, be they 2D or 3D, tend to be more concerned with capturing means than with efforts to represent the range of variation in the corresponding clinical population. In addition, they primarily focus on the face as a whole, whereas some local features may be more informative to distinguish between syndromes. In contrast, the present study introduces a model-driven approach to produce age- and sex-specific estimates of dense syndromic morphology and texture for 95 syndromes. Our model can be used as a detailed reference for visualizing individual syndromic effects, directly comparing the expected morphology between syndromes, and understanding both local and holistic similarities between syndromic phenotypes. The model is available both as an interactive web application and an application programming interface (API) that allows users to apply the syndrome model to their own uses.

Material and methods

Dataset collection

Subjects were enrolled at outpatient clinics and disease-specific patient group meetings in the United States and Canada. The training sample consists of 3,076 individuals comprising 95 syndromes, each represented by 5 or more individuals, as well as 2,273 unrelated non-syndromic individuals. Of these 95 syndromes, 18 have subtypes specified, and within this group, 5 have more than one such subtype represented by sample sizes of 5 or more. Of the 3,076 syndromic individuals, 44.9% were diagnosed with a molecular test while 55.1% have only a clinical diagnosis. The overall sample is ~57.6% female, with ages ranging from <6 months to 78 years old. A by-syndrome breakdown of the sex distribution and age demographics are provided in Table S1.

Enrollment occurred from 2013 to 2023 at both outpatient clinics and rare disease community organization meetings in the United States and Canada. Subjects, or legal guardians when applicable, provided written consent for inclusion in this study. This study involves secondary use of datasets as well as analyses of data obtained by the Hallgrímsson, Spritz, and Klein groups under reviewed protocols that meet ethical standards of the responsible committees on human experimentation (REB14-0340, REB15-1342, University of Calgary).

Nosology

Some syndromes are known to have subtypes associated with different clinical phenotypes. While subtype information may be lacking for some of these, enrolled syndromic subjects overwhelmingly represent the most common subtype. This is the case, for example, for Gaucher disease (MIM: 230800, 230900, 231005) where type 1 (MIM: 230800) represents 95% of the affected population. For other included diagnoses, it may not be obvious why a facial shape phenotype might be present. For example, with polycystic kidney disease (MIM: 173900, 613095, 600666, 61861) it is likely that the vast majority have autosomal dominant polycystic kidney disease (MIM: 173900). While this condition is not classically recognized to have a recognizable facial appearance, prior work in humans and mice has suggested craniofacial effects associated with this disease.[16] Similarly, autism spectrum disorder is a heterogeneous group (390 OMIM entries), and

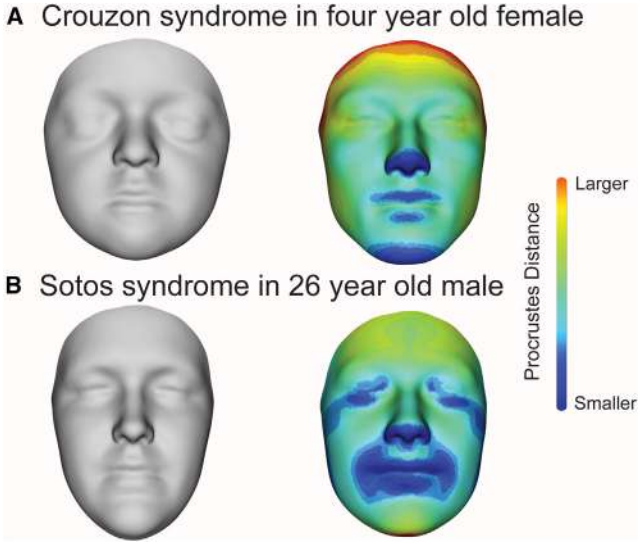

Figure 2. Age- and sex-specific syndrome atlas estimates for Crouzon syndrome and Sotos syndrome
The left column shows the age- and sex-specific estimated facial shape, and the right column shows a heatmap comparison between the syndrome and the age-/sex-matched non-syndromic expectation.

several studies have revealed subtle, if highly varied, facial shape manifestations associated with this phenotypic designation.[17,18]

Mesh processing

We used the 3dMDface stereophotogrammetry scanner to acquire initial 3D facial images for all subjects. We then used an atlas-based approach to non-linearly register each mesh to a common dense mesh topology. The atlas was generated by first choosing a non-syndromic mesh, decimating the mesh to 5,629 vertices, and non-linearly registering ten randomly chosen non-syndromic meshes to the reference 5,629 vertex mesh using the optimal step non-rigid iterative closest point algorithm.[19,20] The final atlas was generated by averaging the registered non-syndromic meshes. The remaining subject meshes were then registered to the average mesh.

Score projection for modeling syndromic severity

Syndromic severity is modeled by projecting principal component scores for a selected syndrome onto the normalized syndrome coefficient vector where the non-syndromic mean shape was used as the model intercept. These scores can be used to estimate a syndromic severity shape component that can be added directly to an age- and sex-specific syndrome estimate. Severity estimates are constrained to 1.5 standard deviations to prevent extrapolation of a shape estimate from the model.

Shape and texture model

The syndromic shape model is fit using multivariate multiple regression. We first reduced the dimensionality of the dense mesh dataset by using only the first 200 principal components of facial shape variation (explaining >99% of the phenotypic variance). We used the principal component axis scores of this principal component analysis (PCA) to model the effects of sex, a cubic effect of age, syndrome, and an age by syndrome interaction as follows:

$$Y \sim \beta_0 + Sex * \beta_{sex} + Age * \beta_{age} + Age^2 * \beta_{age^2} + Age^3 * \beta_{age^3} + Syndrome * \beta_{synd} + Age * Syndrome * \beta_{age*synd} + \varepsilon$$

Y is comprised of principal component scores for shape (x, y, z coordinates).

Model predictions (i.e., syndromic phenotype expectations for various demographic criteria) are initially rendered as axis scores but are then reprojected to 3D coordinates for visualization. For example, Figure 2A depicts an expected 4-year-old female with Crouzon syndrome (MIM: 154400), and Figure 2B shows an expected 26-year-old male with Sotos syndrome (MIM: 117550) derived from the model. Both gestalts are provided with heatmaps describing the differences from an age- and sex-matched non-syndromic estimate.

Real-time registration of novel meshes

The interface facilitates submission of novel facial meshes to compare the morphology of an individual to estimates from the syndrome atlas, as well as submitting a face to an updated version of our previously published syndrome classifier.[9,20] It supports submission of both object replacement character (OBJ) and polygon (PLY) 3D formats with a 50-MB size limit on uploads. Standard facial representations were obtained by registering the atlas to each facial image using the Meshmonk toolbox[21] in Matlab.[22] The atlas was first roughly aligned to each individual image by manually placing 5 positioning landmarks (glabella, pronasale, pogonion, left and right tragion) onto the images. This was followed by rigid and non-rigid registration steps, resulting in homologous correspondence across all 5,629 points.

Imaging and registration errors were detected by measuring deviations from the global mean shape. Procrustes distances were converted to Z scores, and individuals with $Z > 2$ were visually inspected and excluded as needed. The percentage of correspondence outliers (reported by the Meshmonk toolbox) was used as an additional quality control measure.

Application framework

The syndrome atlas uses two core technologies to serve content over the web. Facial archetype shape estimation, calculation of syndrome scores, syndrome classification, and mesh registration are handled using an application programming interface (API). Our API runs as an independent process. Documentation for each function can be accessed at https://genopheno.ucalgary.ca/api/__docs__/. The API was written using the Plumber package in R.[23] The user interface and requests to the API were written in Javascript with BabylonJS used for 3D rendering. The code for the web application, API, as well as a script for making API requests can be found at https://github.com/J0vid/Syndrome_modelJS. A deployable environment is provided for the application in the Github repository using Docker. The provided dockerfile will install a local instance of the syndrome atlas using the official RStudio image as a template (https://hub.docker.com/r/rocker/rstudio). The syndrome atlas can be accessed at https://syndrome-atlas.ca/.

Results

Assessment of model predictions

We assessed model predictions in two ways. First, we calculated each individual's residuals to directly compare each syndromic facial shape to the model's prediction of

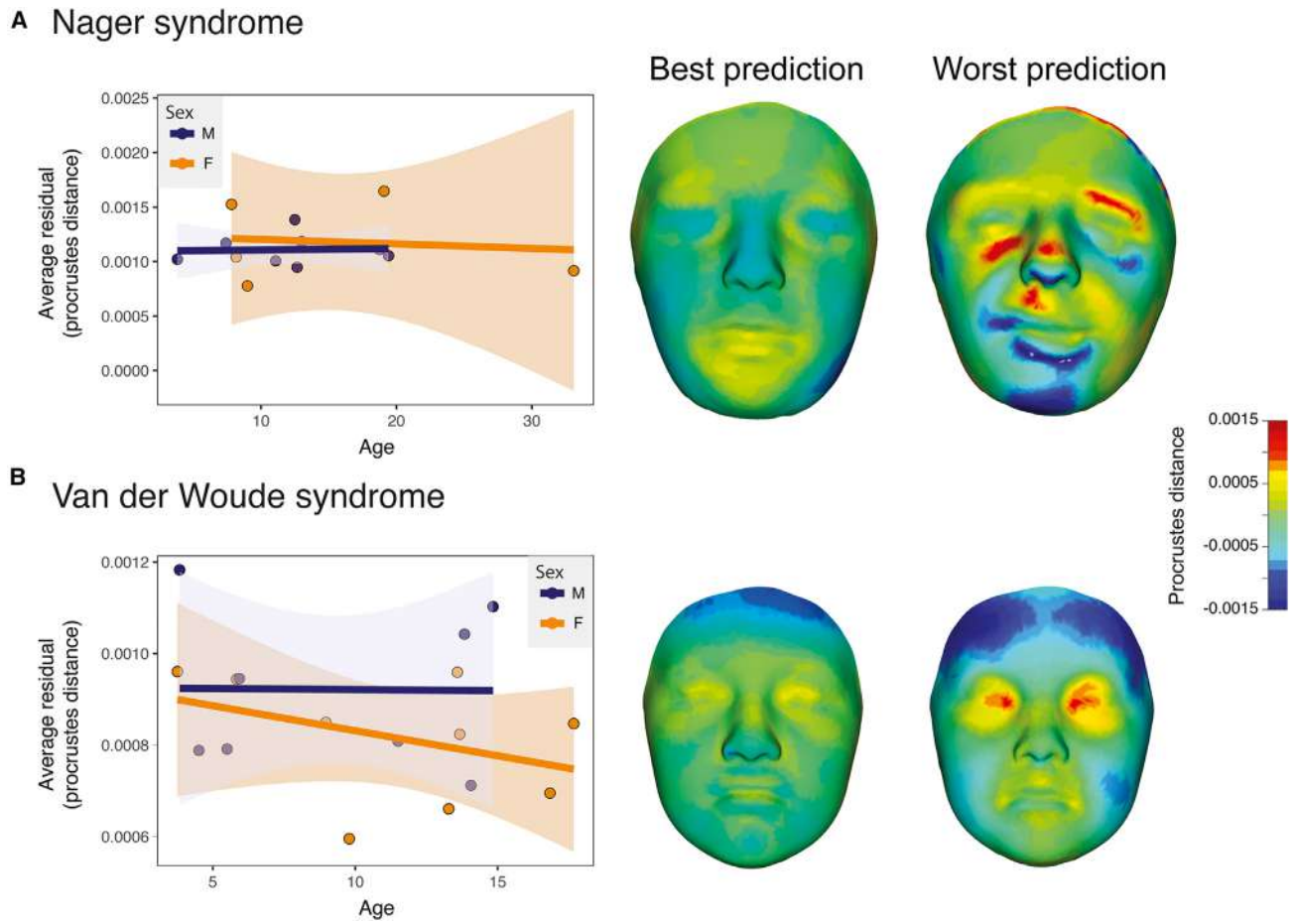

Figure 3. Comparison of age- and sex-matched model predictions for Nager syndrome and Van der Woude syndrome
Each point in the plot represents the mean of the residuals across all mesh vertices for one syndromic individual. The heatmaps represent the differences between the model prediction and an age-, sex-, and syndrome-matched individual for the prediction with the least error (left) and most error (right). The mesh shows the shape of the individuals, and the heatmap colors show the differences to the model estimate with red showing areas that project outwards from the average shape mesh and blue showing areas that project inwards from the mesh.

the expected facial shape for a person of the same age, sex, and syndrome. Figure 3 gives two examples of the residual shape of the best and worst model estimates for Nager syndrome (MIM: 154400) and Van der Woude syndrome (MIM: 119300). These are presented as heatmaps that describe deviations from the expected shape in red and blue colors. Green colors represent areas where the facial shape of the individual closely matches the model predicted shape. The full table of best and worst estimates for each syndrome is provided in Figures S1–S8. The worst demographically matched predictions tend to be syndromic individuals with facial features less typical of their syndrome. For instance, a common deviation from age-matched atlas predictions are individuals with atypically broad chins (see Figures S1 and S7: achondroplasia, Rubinstein-Taybi syndrome [MIM: 180849]).

The second way we evaluated model predictions was to assess the degree to which the model generates realistic instances of the syndromes. This specifically tests for overfitting. One can think of the predicted faces as anonymized representations of the underlying data. If these representations classify poorly by using the classifier that is based on the original data, then the predicted faces are not good anonymized representations. To test this, we estimated how well predicted faces could be classified into their respective diagnostic groups using a classifier trained on real instances of the syndromes. Classification was done using high-dimensional regularized discriminant analysis (HDRDA), which we have previously used to classify syndromic facial shape.[9] To generate simulated faces for classification, we first limited syndromic model estimates to the observed age ranges for each syndrome. We then simulated faces for each syndrome in one-year increments between the minimum and maximum observed age for a syndrome and classified each simulation (Figure 4A). The majority of syndromes classify with 100% sensitivity, suggesting that syndrome model predictions do not produce extreme deviations from their intended syndromic phenotypes, even for age and sex combinations that are not directly observed in the original demographic makeup of the sample. In Figure 4B, we show the relationship between classification

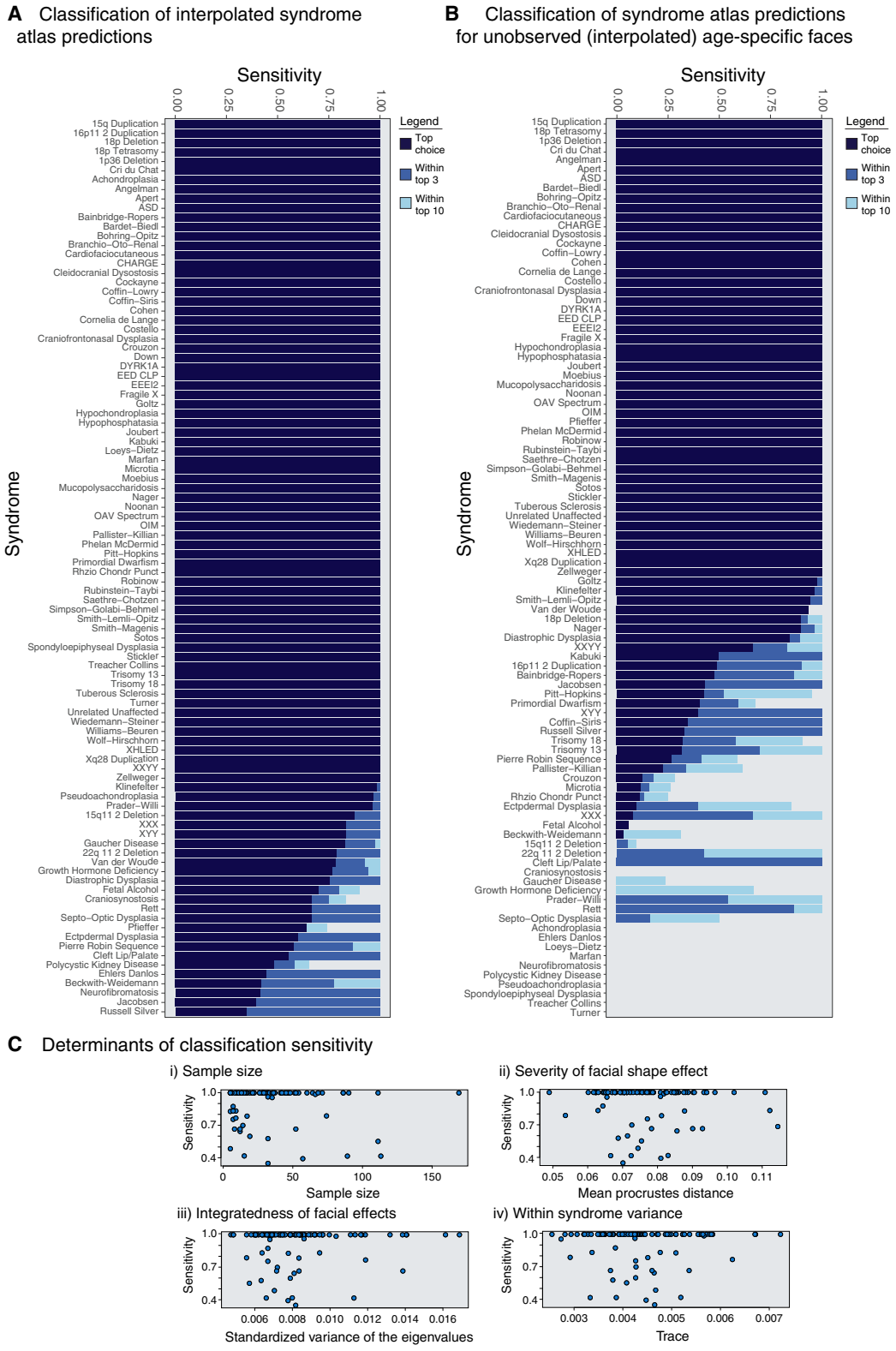

Figure 4. Classification of syndrome atlas predictions and determinants of classification sensitivity

(A) Classification of interpolated syndrome atlas predictions. Predicted shapes for syndromes were constrained to the age range observed for each syndrome and classified.

(B) Classification of syndrome atlas prediction solely for age ranges not observed for each syndrome.

(C) Relationship between classification sensitivity and sample size, average Procrustes distance to the non-syndromic mean face, the standardized variance of the eigenvalues, and the trace of the covariance matrix for each syndrome. Procrustes distance measures shape differences among configurations of landmark coordinates. The variance of eigenvalues measures the extent to which variation in shape is concentrated on the first few principal components. Each point represents an individual syndrome.

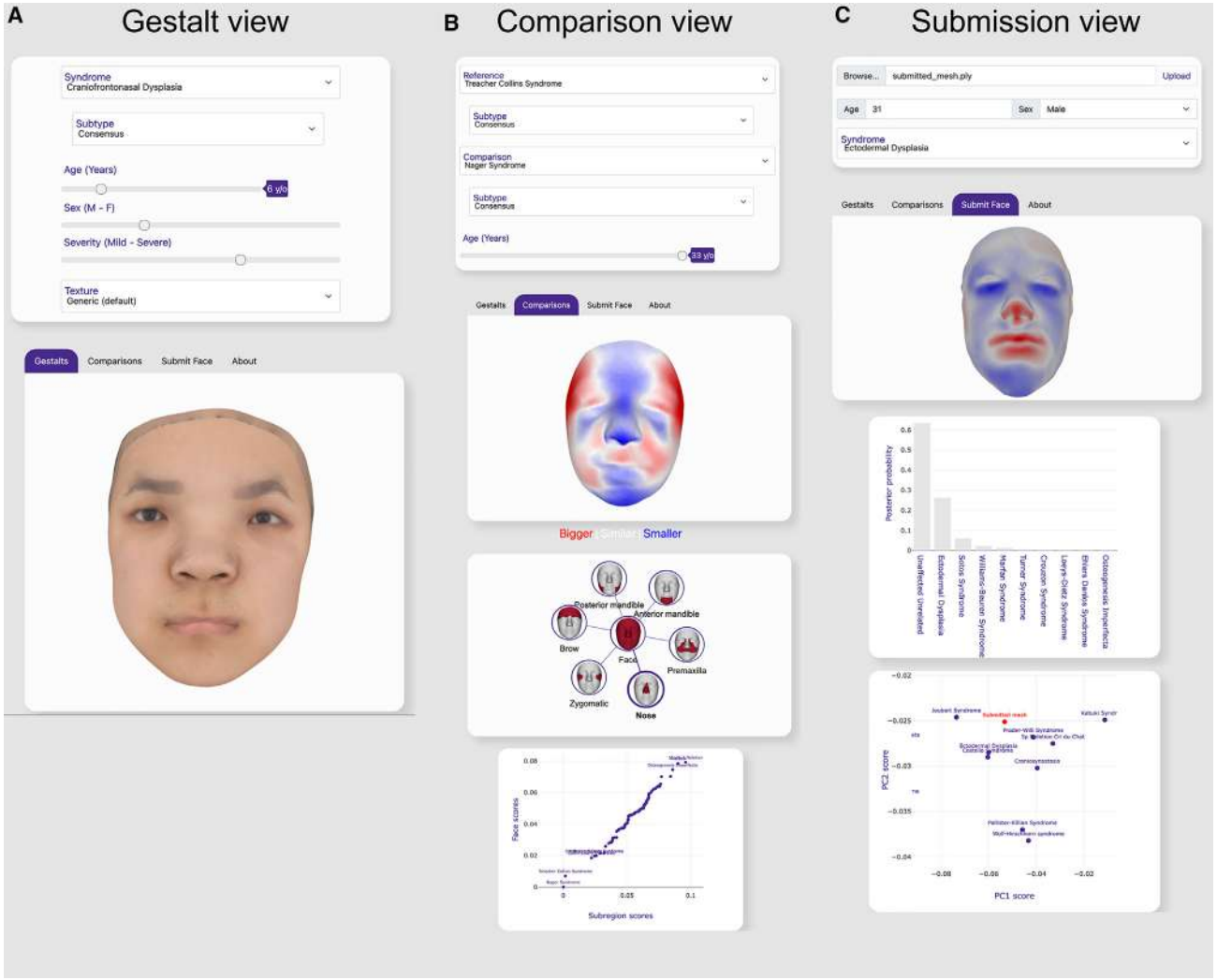

Figure 5. Panel views of the syndrome atlas application

The application supports a mobile view driven by touch interactions (A–C) as well as a desktop view with mouse/keyboard controls (Figures S9–S11).

(A) The gestalt tab focuses on individual syndrome visualization. Here we see an estimated face that would correspond to a 6-year-old male with severe craniofrontonasal dysplasia.

(B) The comparison tab allows for the comparison between any syndrome or non-syndromic group. Comparisons can be limited to subsets of the facial morphology shown in the bottom box. The morphospace plot on the bottom shows the similarity of all syndromes to the specified syndrome.

(C) The submitted face tab allows for the submission and registration of a novel mesh. The registered mesh is then run through a syndrome classifier (middle row) and projected onto syndromic principal component axes (bottom row). In the principal component space, the registered mesh is highlighted among age- and sex-matched projected atlas predictions for each syndrome.

sensitivity and various properties of each syndrome. Classification of syndrome atlas estimates is generally not associated with the sample size, severity, integratedness, or variance of the syndrome. This suggests that the model is robust to biases due to low syndrome sample size or to syndromes with extreme phenotypes and high variability. Figure 4C focuses on classifying syndrome atlas predictions for extrapolated age ranges for each syndrome. Classification for many syndromes is poor when extrapolated to more extreme unobserved age ranges, suggesting that there may be non-linear or unique age-by-syndrome interactions that require higher sample size to model more accurately.

Web-based atlas of syndrome morphology

Finally, we have developed an atlas of syndromic morphology web application, which may be of use to the clinical and academic community. The application is organized into three sections: gestalts, comparisons, and submitted face.

The gestalt visualizations (Figure 5A) are interactive. They can be rotated and zoomed using a mouse on a desktop or with touch input on a mobile device. The gestalt visualizations are also dynamic with respect to age, sex, and severity. For syndrome subtypes with at least 5 observations, we provide additional visualization options. The default is a consensus gestalt that pools all

observations for that syndrome. The second is an unspecified subtype which provides an estimate from only individuals with unknown subtypes. Finally, we provide individual subtypes unique to each syndrome.

When a syndrome is selected, a gestalt for a specific age-sex combination is automatically generated. Age can be modified by dragging the age slider manually or by entering a specific age. To avoid extrapolation beyond the observed data, each syndrome's selectable age range and sex is determined by the syndrome sample composition (Table S1).

The syndrome web application also includes features for visualizing within-syndrome phenotypic heterogeneity. In general, syndromic faces are more variable than non-syndromic faces, and heterogeneity itself is a characteristic feature of syndromic facial morphology.[9,15] To illustrate heterogeneity, the application allows the user to modify the severity of the syndromic phenotype. For a given syndrome, severity is defined by the range of variation of syndromic individuals along the axis through shape space that passes through the mean shape for the syndrome. Individuals that are more severe than the mean will have residual shapes that score higher along the syndromic vector. Like age parameters, the magnitude of modifiable severity is determined by the range of syndromic severities observed in the sample. A selected syndrome visualization can be made 1.5 standard deviations more mild or more severe using the severity slider.

Gestalts can be displayed with or without texture. By default, the syndrome application uses one of nine selectable generic skin textures. Three-dimensional visualizations of syndrome morphology have traditionally been presented without skin texture to maintain the privacy of the participants that have been scanned. We aimed to generate useful texture visualizations that are derived from the diversity of skin texture in our dataset without relying on any one individual. To do so, we measured mesh texture by registering the texture images of a small sample of meshes for each syndrome, producing texture images with UV correspondence to the dense registered mesh. We then generated novel synthetic textures by averaging textures within syndromes. Figure 5A shows a gestalt of a 6-year-old male with severe craniofrontonasal dysplasia (MIM: 304110) with the default generic skin texture applied.

The second section of the syndrome atlas is the "comparisons" tab. The features in the comparisons tab allow users to visualize quantitative morphological differences between any two syndromic estimates, as well as to an age- and sex-matched non-syndromic equivalent. Comparisons are displayed with a heatmap, which uses red colors to represent local expansion and blue colors to denote local contraction; white shades denote areas of shape similarity between the two estimates. This feature may be particularly useful for understanding trajectories of facial phenotypes for syndromes that tend to produce similar characteristic features during some parts of development. For example, Figure 5B compares a 33-year-old male with Nager syndrome (MIM: 154400) estimate to an age- and sex-matched Treacher Collins syndrome (MIM: 154500, 248390, 613717) estimate. Users can visualize differences in pre-defined specific facial regions of interest (Figure 5B, bottom box); the comparison in Figure 5B focuses on nasal morphology. The heatmap is updated in real-time as the age slider changes, allowing users to see how the difference between syndromes changes with age.

To compare a syndrome of interest to multiple syndromes simultaneously, the comparisons tab includes a plot that summarizes shape information across the dataset for the selected syndrome (Figure 5B). Each data point in the plot represents the average projected scores for each syndrome along the selected syndrome coefficient vector. The five most similar syndromes are labeled. When a morphological subset is selected, the average similarity score for each syndrome to the selected syndrome in the selected subset is provided on the x axis. The y axis always provides full face scores for reference.

The third component of the syndrome atlas can be found under the "submitted face" tab (Figure 5C). This tab allows for the submission of novel meshes with age and sex covariates that will be registered to the syndrome atlas. There are several analysis options for a submitted mesh. The first is the ability to make direct comparisons, presented as a heatmap, to any age- and sex-matched syndromic estimate in order to identify which syndromes have the most similar phenotype to the mesh. We also provide an estimate of the syndrome classification probabilities for the mesh with an updated version of our previously published classifier with 82 syndrome classes.[9] Finally, we provide a scatterplot showing the position of the submitted face shape (highlighted in red) in the principal component shape space of the syndromic dataset.

Discussion

Medical geneticists have long relied on facial features as a component of clinical diagnosis. In practice, this can range from informal clinical gestalt to structured use of deep phenotyping methods such as phenotype ontologies[24] or quantitative classification based on two- or three-dimensional facial images.[9,20,25] Here, we leverage the growing database of 3D facial images of individuals with rare disease diagnoses to create an online reference tool to aid clinical diagnosis. This tool is intended to provide a systematic representation of the facial shape effects associated with genetic diseases. It also allows clinicians to visualize variation in manifestation and severity of those facial shape effects as well as their interactions with sex and age.

Quantitative gestalts, such as those that we provide here, are only as representative as the underlying data that have been collected (see Table S1 for a demographic summary of the dataset used herein). Our current dataset is of overwhelmingly European ancestry and thus has as-yet

unknown generalizability to other ethnicities. Moreover, the syndromes represented in the dataset are rare in the population at large. It is challenging to collect enough syndromic examples across their full range of ages and ethnicities to confidently estimate an age- or ethnicity-specific gestalt. This limitation can be mitigated if there are no strong age/ethnicity-by-syndrome phenotypic interactions. While recent concerted efforts to expand our understanding of the relationship between syndromic facial phenotypes and ethnicity are a step in the right direction, most utilize 2D images.[26] Our prior work does not reveal significant race or ethnicity effects on overall classification accuracy from facial shape.[9] This does not mean, however, that there might not be significant interactions that could affect accuracy for individual syndromes. International collaboration focused on the collection of 3D facial images from syndromic subjects of diverse racial and ethnic backgrounds should be a greater priority in the future.

The syndrome gestalt model presented here also does not explicitly model asymmetric aspects of craniofacial syndromes. This should not affect classification efforts for syndromes in which the asymmetry is randomly distributed between the left and right sides of the face (e.g., Cornelia de Lange syndrome[27] [MIM: 122470]), since these deviations will tend to cancel out in the overall analysis. However, in syndromes in which asymmetry is consistently sided (directional asymmetry), such as with oculoauriculovertebral spectrum (MIM: 164210), that asymmetry will tend not to be exploited for its diagnostic value in our model.

The ability to submit novel faces to the syndrome atlas raises several considerations. The first pertains to the comparison of an individual's facial morphology to the syndrome atlas. Upon registration of a face to a homologous topology, we project the face into the principal component space of our dataset. We then show the individual's similarity to others in the dataset as a reference for where their face resides in the atlas of syndromic morphology. It is important to note that the combined effects of sex, age, syndrome, allometry, and ethnicity all contribute to the variation in the atlas. One must take care not to interpret a subject's location in the space solely as a syndromic effect. There is substantial facial shape heterogeneity in syndromic directions even in non-syndromic populations,[28,29] so similarity to syndromic morphology should not automatically be assumed to imply potential syndromic genetic mutations. This is equally true when interpreting the results of the syndromic classifier. Facial shape with no additional contextual information may be useful for delineating a set of potential syndromes for further validation, but it should not be used as a substitute for genetic screening, clinical assessment, and testing. Machine learning algorithms may incorrectly classify an individual as syndromic when they do not have a genetic syndrome, and they may incorrectly classify an individual with a syndrome as non-syndromic. It is possible the occurrence of such false positives and false negatives would be exacerbated by ethnic and other demographic insufficiencies present in the training data. There is a history of sex and ethnic bias in facial recognition algorithms, so syndrome classification algorithms that rely on facial shape from images and 3D scans may be susceptible to analogous problems.[30,31]

The aim of this work is to provide a detailed reference for the characteristic phenotypes of craniofacial syndromes for clinical geneticists. Phenotyping continues to be integral to clinical assessment because of its utility for diagnosis. This tool is positioned as a reference tool for clinicians to visualize specific syndromic presentation. It is also a powerful tool for the comparison of an individual's morphology to demographically matched syndrome visualizations. Current methods for automated syndrome classification require clinician interpretation, emphasizing the continued need for phenotype references. Aids that provide context for the clinician's needs are increasingly important for diagnosis. Finally, there is substantial promise in expanding the utility of the syndrome atlas by targeted collection of ethnically diverse additional syndromic facial shape data.

Data and code availability

All of the primary data used to create the syndrome atlas application are shared via Facebase (accession numbers FB00000861 [https://doi.org/10.25550/TJ0], FB00000892 [https://doi.org/10.25550/TK0], and FB00000491 [https://doi.org/10.25550/VWP]). Code is available at https://github.com/J0vid/Syndrome_modelJS. The exception to this is the optimized code for mesh upload and registration as this is proprietary to DeepSurfaceAI.

Supplemental information

Supplemental information can be found online at https://doi.org/10.1016/j.ajhg.2023.11.011.

Acknowledgments

This project was supported by NIH-NIDCR grant U01DE024440 to R.A.S., O.D.K., and B.H.; a CIHR Foundation grant to B.H.; the Alberta Children's Hospital Foundation; and a Canada First Research Excellence Fund Grant (CFREF 2022-00015) to B.H. and F.P.B.

Declaration of interests

J.D.A., D.C.K., T.C., and J.H.M.P. are employees of DeepSurfaceAI, a company that uses 3D facial imaging and analysis to develop software that aids plastic craniofacial surgery. J.D.A., J.J.B., D.C.K., N.D.F., and B.H. have a financial stake in this company. DeepSurfaceAI is not currently engaged in the use of facial imaging for syndrome diagnosis and has no immediate plans to do so.

Received: June 3, 2023
Accepted: November 29, 2023
Published: January 4, 2024

References

1. Hart, T.C., and Hart, P.S. (2009). Genetic studies of craniofacial anomalies: clinical implications and applications. Orthod. Craniofac. Res. *12*, 212–220.
2. Yang, Y., Muzny, D.M., Xia, F., Niu, Z., Person, R., Ding, Y., Ward, P., Braxton, A., Wang, M., Buhay, C., et al. (2014). Molecular findings among patients referred for clinical whole-exome sequencing. JAMA *312*, 1870–1879.
3. Vincent, M., Geneviève, D., Ostertag, A., Marlin, S., Lacombe, D., Martin-Coignard, D., Coubes, C., David, A., Lyonnet, S., Vilain, C., et al. (2016). Treacher Collins syndrome: a clinical and molecular study based on a large series of patients. Genet. Med. *18*, 49–56.
4. Ramos, F.J., Puisac, B., Baquero-Montoya, C., Gil-Rodríguez, M.C., Bueno, I., Deardorff, M.A., Hennekam, R.C., Kaiser, F.J., Krantz, I.D., Musio, A., et al. (2015). Clinical utility gene card for: Cornelia de Lange syndrome. Eur. J. Hum. Genet. *23*, 1431.
5. Cocciadiferro, D., Augello, B., De Nittis, P., Zhang, J., Mandriani, B., Malerba, N., Squeo, G.M., Romano, A., Piccinni, B., Verri, T., et al. (2018). Dissecting KMT2D missense mutations in Kabuki syndrome patients. Hum. Mol. Genet. *27*, 3651–3668.
6. Acke, F.R., Malfait, F., Vanakker, O.M., Steyaert, W., De Leeneer, K., Mortier, G., Dhooge, I., De Paepe, A., De Leenheer, E.M.R., and Coucke, P.J. (2014). Novel pathogenic COL11A1/COL11A2 variants in Stickler syndrome detected by targeted NGS and exome sequencing. Mol. Genet. Metab. *113*, 230–235.
7. Basel-Vanagaite, L., Wolf, L., Orin, M., Larizza, L., Gervasini, C., Krantz, I.D., and Deardoff, M.A. (2016). Recognition of the Cornelia de Lange syndrome phenotype with facial dysmorphology novel analysis. Clin. Genet. *89*, 557–563.
8. Muenke, M., Adeyemo, A., and Kruszka, P. (2016). An electronic atlas of human malformation syndromes in diverse populations. Genet. Med. *18*, 1085–1087.
9. Hallgrímsson, B., Aponte, J.D., Katz, D.C., Bannister, J.J., Riccardi, S.L., Mahasuwan, N., McInnes, B.L., Ferrara, T.M., Lipman, D.M., Neves, A.B., et al. (2020). Automated syndrome diagnosis by three-dimensional facial imaging. Genet. Med. *22*, 1682–1693.
10. Matthews, H.S., Palmer, R.L., Baynam, G.S., Quarrell, O.W., Klein, O.D., Spritz, R.A., Hennekam, R.C., Walsh, S., Shriver, M., Weinberg, S.M., et al. (2021). Large-scale open-source three-dimensional growth curves for clinical facial assessment and objective description of facial dysmorphism. Sci. Rep. *11*, 12175.
11. Bannister, J.J., Wilms, M., Aponte, J.D., Katz, D.C., Klein, O.D., Bernier, F.P.J., Spritz, R.A., Hallgrimsson, B., and Forkert, N.D. (2022). A Deep Invertible 3D Facial Shape Model For Interpretable Genetic Syndrome Diagnosis. IEEE J. Biomed. Health Inform. *26*, 3229–3239.
12. Deutsch, C.K., Shell, A.R., Francis, R.W., and Bird, B.D. (2012). The Farkas system of craniofacial anthropometry: methodology and normative databases. In Handbook of anthropometry: Physical measures of human form in health and disease, pp. 561–573.
13. Ferry, Q., Steinberg, J., Webber, C., FitzPatrick, D.R., Ponting, C.P., Zisserman, A., and Nellåker, C. (2014). Diagnostically relevant facial gestalt information from ordinary photos. Elife *3*, e02020.
14. Hammond, P., Hutton, T.J., Allanson, J.E., Campbell, L.E., Hennekam, R.C.M., Holden, S., Patton, M.A., Shaw, A., Temple, I.K., Trotter, M., et al. (2004). 3D analysis of facial morphology. Am. J. Med. Genet. *126A*, 339–348.
15. Hammond, P. (2007). The use of 3D face shape modelling in dysmorphology. Arch. Dis. Child. *92*, 1120–1126.
16. Khonsari, R.H., Ohazama, A., Raouf, R., Kawasaki, M., Kawasaki, K., Porntaveetus, T., Ghafoor, S., Hammond, P., Suttie, M., Odri, G.A., et al. (2013). Multiple postnatal craniofacial anomalies are characterized by conditional loss of polycystic kidney disease 2 (Pkd2). Hum. Mol. Genet. *22*, 1873–1885.
17. Boutrus, M., Maybery, M.T., Alvares, G.A., Tan, D.W., Varcin, K.J., and Whitehouse, A.J.O. (2017). Investigating facial phenotype in autism spectrum conditions: The importance of a hypothesis driven approach. Autism Res. *10*, 1910–1918.
18. Sleyp, Y., Matthews, H., Vanneste, M., Vandenhove, L., Hoskens, H., Indencleef, K., Steyaert, J., Devriendt, K., Claes, P., and Peeters, H. (2022). The Potential of 3D Facial Analysis to Recognize Monogenic Autism in the Spectrum, p. 30.
19. Amberg, B., Romdhani, S., and Vetter, T. (2007). Optimal Step Nonrigid icp Algorithms for Surface Registration (IEEE), pp. 1–8.
20. Bannister, J.J., Crites, S.R., Aponte, J.D., Katz, D.C., Wilms, M., Klein, O.D., Bernier, F.P.J., Spritz, R.A., Hallgrímsson, B., and Forkert, N.D. (2020). Fully Automatic Landmarking of Syndromic 3D Facial Surface Scans Using 2D Images. Sensors *20*, 3171.
21. White, J.D., Indencleef, K., Naqvi, S., Eller, R.J., Hoskens, H., Roosenboom, J., Lee, M.K., Li, J., Mohammed, J., Richmond, S., et al. (2021). Insights into the genetic architecture of the human face. Nat. Genet. *53*, 45–53.
22. Inc, T.M. (2022). MATLAB versionm 9.13.0 (The MathWorks Inc.).
23. Schloerke, B., and Allen, J. (2021). plumber: An API Generator for R Package. version 1.1. 0.
24. Köhler, S., Vasilevsky, N.A., Engelstad, M., Foster, E., McMurry, J., Aymé, S., Baynam, G., Bello, S.M., Boerkoel, C.F., Boycott, K.M., et al. (2016). The Human Phenotype Ontology in 2017. Nucleic Acids Res. *45*, D865–D876.
25. Gurovich, Y., Hanani, Y., Bar, O., Nadav, G., Fleischer, N., Gelbman, D., Basel-Salmon, L., Krawitz, P.M., Kamphausen, S.B., Zenker, M., et al. (2019). Identifying facial phenotypes of genetic disorders using deep learning. Nat. Med. *25*, 60–64.
26. Kruszka, P., Tekendo-Ngongang, C., and Muenke, M. (2019). Diversity and dysmorphology. Curr. Opin. Pediatr. *31*, 702–707.
27. Kline, A.D., Moss, J.F., Selicorni, A., Bisgaard, A.-M., Deardorff, M.A., Gillett, P.M., Ishman, S.L., Kerr, L.M., Levin, A.V., Mulder, P.A., et al. (2018). Diagnosis and management of Cornelia de Lange syndrome: first international consensus statement. Nat. Rev. Genet. *19*, 649–666.
28. Hoskens, H., Claes, P., Peeters, H., and Hens, G. (2021). The Complex Facial Phenotype: New Approaches in Family-Based Studies.
29. Liu, F., Van Der Lijn, F., Schurmann, C., Zhu, G., Chakravarty, M.M., Hysi, P.G., Wollstein, A., Lao, O., De Bruijne, M., Ikram, M.A., et al. (2012). A genome-wide association study identifies five loci influencing facial morphology in Europeans. PLoS Genet. *8*, e1002932.
30. Buolamwini, J., and Gebru, T. (2018). Gender Shades: Intersectional Accuracy Disparities in Commercial Gender Classification (PMLR), pp. 77–91.
31. Castelvecchi, D. (2020). Is facial recognition too biased to be let loose? Nature *587*, 347–349.